PERGAMON

Chemical Engineering Science 57 (2002) 1849–1858

Chemical Engineering Science

www.elsevier.com/locate/ces

Transverse migration of single bubbles in simple shear flows

Akio Tomiyama[a,*], Hidesada Tamai[a], Iztok Zun[b], Shigeo Hosokawa[a]

[a] *Graduate School of Science and Technology, Kobe University, Rokkodai, Nada, Kobe 657-8501, Japan*
[b] *Faculty of Mechanical Engineering, University of Ljubljana, Askerceva 6, 1000, Ljubljana, Slovenia*

Received 24 October 2001; received in revised form 18 February 2002; accepted 20 February 2002

Abstract

Trajectories of single air bubbles in simple shear flows of glycerol–water solution were measured to evaluate transverse lift force acting on single bubbles. Experiments were conducted under the conditions of $-5.5 \leqslant \log_{10} M \leqslant -2.8$, $1.39 \leqslant Eo \leqslant 5.74$ and $0 \leqslant |\mathrm{d}V_L/\mathrm{d}y| \leqslant 8.3\ \mathrm{s}^{-1}$, where M is the Morton number, Eo the Eötvös number and $\mathrm{d}V_L/\mathrm{d}y$ the velocity gradient of the shear flow. A net transverse lift coefficient C_T was evaluated by making use of all the measured trajectories and an equation of bubble motion. It was confirmed that C_T for small bubbles is a function of the bubble Reynolds number Re, whereas C_T for larger bubbles is well correlated with a modified Eötvös number Eo_d which employs the maximum horizontal dimension of a deformed bubble as a characteristic length. An empirical correlation of C_T was therefore summarized as a function of Re and Eo_d. The critical bubble diameter causing the radial void profile transition from wall peaking to core peaking in an air–water bubbly flow evaluated by the proposed C_T correlation coincided with available experimental data.

Keywords: Multiphase flow; Bubble; Lateral migration; Lift force; Simple shear flow

1. Introduction

Accurate prediction of developing bubble flows in vertical pipes cannot be carried out without sufficient knowledge of a transverse lift force acting on a bubble, the force which governs the direction of transverse migration of a bubble in a shear field. It has been clarified through a number of experiments that the lateral migration strongly depends on bubble size, i.e., small bubbles tend to migrate toward the pipe wall which causes a wall-peak bubble distribution, whereas large bubbles tend to migrate toward the pipe center which results in a core-peak bubble distribution. For an air–water system at atmospheric pressure and room temperature, bubbles ranging from about 1 to 5 mm in sphere-volume equivalent diameter d might correspond to small bubbles, and bubbles larger than about 5 mm to large bubbles (Liu, 1993; Grossetete, 1995; Sakaguchi, Ijiri, Tabasaki, & Shakutsui, 1996).

The migration of small bubbles toward the pipe wall can be explained with the so-called shear-induced lift force model (Zun, 1980; Auton, 1987; Drew and Lahey, 1987) given by

$$\boldsymbol{F}_{LF} = -C_{LF}\rho_L \frac{\pi d^3}{6}(\boldsymbol{V}_G - \boldsymbol{V}_L) \times \mathrm{rot}\, \boldsymbol{V}_L, \tag{1}$$

where the subscripts G and L denote the gas and liquid phases, respectively, $\boldsymbol{F}_{LF}$ is the shear-induced lift force, C_{LF} the lift coefficient, ρ the density and $\boldsymbol{V}$ the velocity. Zun (1980) and Lance and Lopez de Berodano (1994) reported that C_{LF} for small bubbles in an air–water system takes a value ranging from 0.25 to 0.3. As for the migration toward the pipe center, Serizawa and Kataoka (1994) surveyed available experimental data and presumed that the direction of lateral migration would be governed by complex interaction between a bubble wake and a shear field about the bubble. The validity of their presumption was partly confirmed by Tomiyama, Zun, Sou, and Skaguchi (1993) and Tomiyama, Sou, Zun, Kanami, and Sakaguchi (1995). They carried out interface tracking simulation of single bubbles in a Poiseuille flow and pointed out that the migration toward the pipe center relates to the presence of a slanted wake behind a deformed bubble, which is apparently caused by the interaction between the wake and shear field. In addition,

* Corresponding author. Fax: +81-78-803-1131.
E-mail address: tomiyama@mech.kobe-u.ac.jp (A. Tomiyama).

0009-2509/02/$ - see front matter
PII: S0009-2509(02)00085-4

their simulation indicated that another kind of transverse lift force, $\boldsymbol{F}_{TL}$, is induced by the complex interaction.

In spite of these previous studies, our knowledge on the lateral migration is still insufficient due to the lack of relevant experimental data. Fundamental experiments on lateral migration such as the measurement of bubble trajectories in a simple shear flow conducted by Kariyasaki (1987) are definitely indispensable for improving transverse lift force models. Trajectories of single air bubbles in simple shear flows of viscous liquids were therefore measured in this study to provide an experimental database and to present an empirical correlation of a net transverse lift force. The applicability of the proposed correlation to bubbles in low liquid viscosity systems was also discussed.

2. Experiments

The Morton number M, which is a property group of the two phases, the Eötvös number Eo, which is the ratio of buoyancy to surface tension forces, and the intensity of a velocity gradient ω of a simple shear flow were selected as the parameters of experiments. They are defined by

$$M = \frac{g(\rho_L - \rho_G)\mu_L^4}{\rho_L^2 \sigma^3}, \tag{2}$$

$$Eo = \frac{g(\rho_L - \rho_G)d^2}{\sigma} \tag{3}$$

and

$$\omega = |\mathrm{rot}\, \boldsymbol{V}_L| = \left|\frac{\mathrm{d}V_L}{\mathrm{d}y}\right|, \tag{4}$$

respectively. Here g denotes the acceleration of gravity, μ the viscosity, σ the surface tension, $\boldsymbol{V}_L$ the liquid velocity in the vertical (z) direction and y the horizontal coordinate. Note that in the case of a two-dimensional simple shear flow heading in the z direction, the x, y and z components of the liquid velocity vector $\boldsymbol{V}_L$ are given by $(0, 0, V_L(y))$, and thereby the liquid velocity gradient $\omega = |\mathrm{d}V_L/\mathrm{d}y|$ is equivalent to $|\mathrm{rot}\, \boldsymbol{V}_L|$. These quantities were varied within the ranges of $-5.5 \leqslant \log_{10} M \leqslant -2.8$, $1.39 \leqslant Eo \leqslant 5.74$ and $0 \leqslant \omega \leqslant 8.3\ \mathrm{s}^{-1}$.

Fig. 1 shows a schematic of the experimental setup. Glycerol–water solution at atmospheric pressure and room temperature was filled in the acrylic tank, the height, width and depth of which were 0.9, 0.45 and 0.152 m, respectively. The seamless belt, 0.15 m in width, was rotated by the servomotor at a constant speed, the value of which was regulated by a controller within the range of 0–0.27 m/s. The position of the rotating belt was stabilized by the two guide plates and two pulleys so as to prevent its bending and fluttering. A simple shear flow with a constant velocity gradient ω was thus realized in the 0.03 m gap between the belt and sidewall of the tank. Distilled water was used for making the glycerol–water solution to avoid the effect of

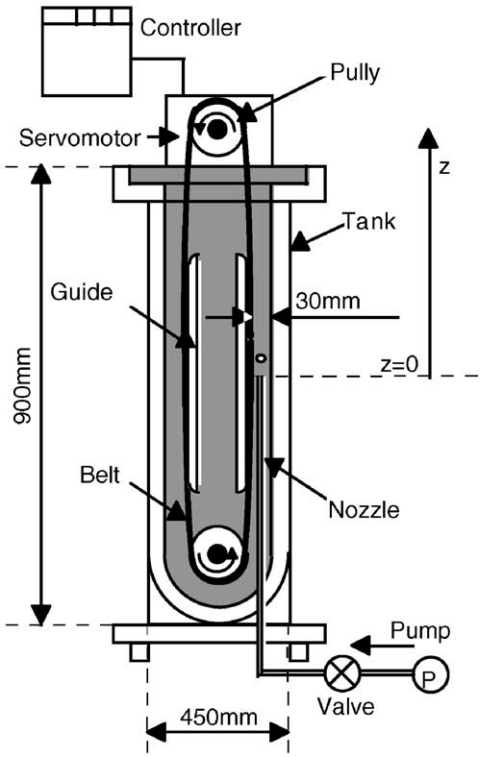

Fig. 1. Schematic of experimental apparatus.

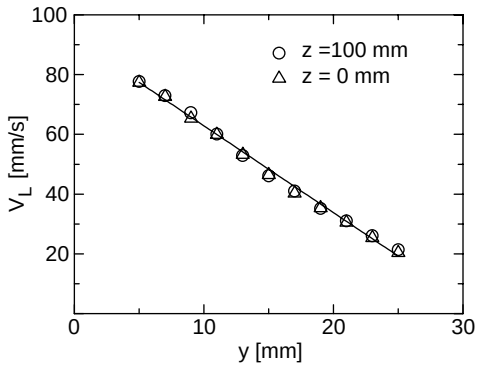

Fig. 2. An example of measured liquid velocity profiles.

surfactants on lateral migration. A single air bubble was released from a nozzle made of a brass tube. The nozzle tip was positioned at the elevation where the liquid flow established a simple shear flow. Fig. 2 is an example of liquid velocity profiles measured with a hot film probe at the nozzle location ($z = 0$ m) and at 0.1 m downstream of the nozzle location ($z = 0.1$ m). Five different tubes with 0.14, 0.5, 2.0, 3.0 and 4.0 mm in inside diameter were used for the nozzle to release various bubbles. The liquid density was evaluated as the ratio of a measured mass of the solution to its volume. The liquid viscosity and surface tension were measured with a rotational viscometer and a capillary tube tensiometer, respectively. Bubble shapes and trajectories were recorded using a high-speed video camera (shutter speed = 1/1000 s, frame rate = 400 frame/s). Enlarged video images were used

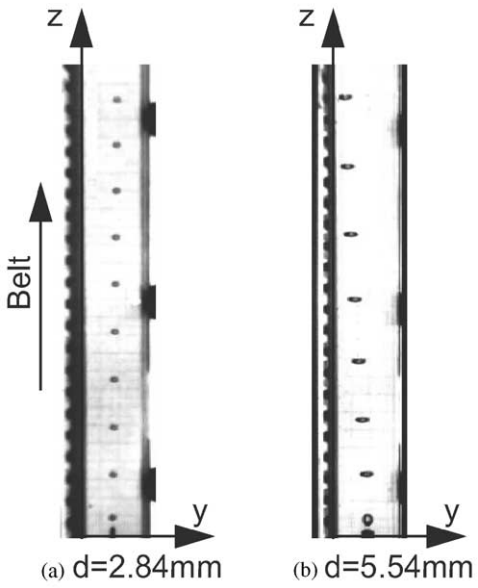

Fig. 3. Two examples of consecutive images of single bubbles in a simple shear flow: $\log_{10} M = -5.3$, $\omega = 3.8\ \mathrm{s}^{-1}$.

to evaluate d and its aspect ratio. The uncertainties estimated at 95% confidence for measured ρ_L, μ_L, σ, d and ω were 0.6%, 2.0%, 3.3%, 0.7% and 2.3%, respectively. The measurement error of bubble position was ±0.3 mm. All the measured fluid properties are summarized in Table 1 in the appendix.

Fig. 3 shows two examples of consecutive images of single bubbles in a shear flow. The small bubble in Fig. 3(a) migrated toward the stationary sidewall, whereas the large bubble in Fig. 3(b) migrated toward the moving belt. Similar images were taken for various combinations of d, ω and M. As a result, a database consisting of 116 trajectories was obtained. As an example, a dataset for $\log_{10} M = -5.3$ is shown in Fig. 4. The data for the other Morton number systems are summarized in the appendix. The y^* and z^* in the figure are the dimensionless horizontal and vertical coordinates, normalized by the gap width $D = 30$ mm, i.e., $y^* = y/D$ and $z^* = z/D$. This figure clearly shows that (1) the direction of lateral migration under a constant Morton number is not affected by ω, but by the bubble diameter d, in other words, by the Eötvös number Eo, and (2) the lateral migration length increases with ω. As shown in Figs. 11 and 12 in the appendix, bubbles in the other Morton number systems exhibited the same tendencies.

3. Evaluation of lift coefficient under a simple shear flow

Bubble trajectories were calculated using a one-way bubble tracking method to evaluate the transverse lift force acting on a bubble. Since the measured lateral migration length was proportional to ω both for the bubbles migrating toward the moving belt and for the bubbles migrating toward the stationary wall, it was assumed in the calculations that $\boldsymbol{F}_{TL}$ caused by the slanted wake has the same functional form as that of the shear-induced lift force $\boldsymbol{F}_{LF}$, that is,

$$\boldsymbol{F}_{TL} = -C_{TL}\rho_L \frac{\pi d^3}{6}(\boldsymbol{V}_G - \boldsymbol{V}_L) \times \mathrm{rot}\, \boldsymbol{V}_L, \tag{5}$$

where C_{TL} is the transverse lift coefficient due to the slanted wake. Hence the net transverse lift force $\boldsymbol{F}_T$ was assumed to be given by

$$\boldsymbol{F}_T = \boldsymbol{F}_{LF} + \boldsymbol{F}_{TL} = -(C_{LF} + C_{TL})\rho_L \frac{\pi d^3}{6}(\boldsymbol{V}_G - \boldsymbol{V}_L) \times \mathrm{rot}\, \boldsymbol{V}_L$$

$$= -C_T \rho_L \frac{\pi d^3}{6}(\boldsymbol{V}_G - \boldsymbol{V}_L) \times \mathrm{rot}\, \boldsymbol{V}_L, \tag{6}$$

where C_T is the net transverse lift coefficient, i.e. the sum of shear- and wake-induced lift coefficient.

The equation of bubble motion was therefore given by

$$(\rho_G + 0.5\rho_L)\frac{\mathrm{d}\boldsymbol{V}_G}{\mathrm{d}t} = -\frac{3C_D\rho_L}{4\mathrm{d}}|\boldsymbol{V}_R|\boldsymbol{V}_R - C_T\rho_L\boldsymbol{V}_R \times \mathrm{rot}\, \boldsymbol{V}_L + (\rho_L - \rho_G)\boldsymbol{g}, \tag{7}$$

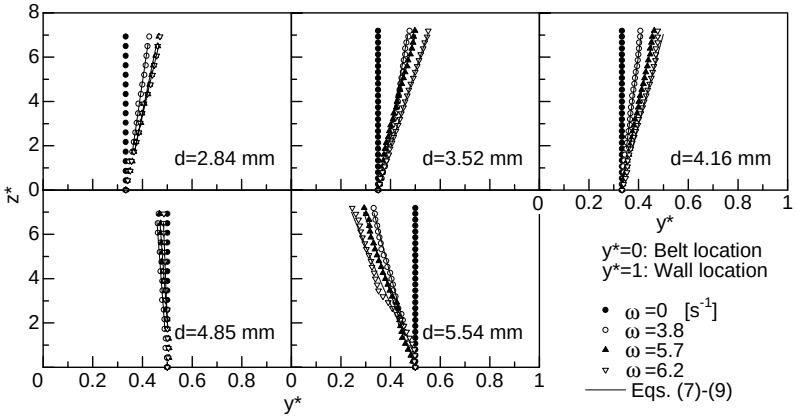

Fig. 4. Measured bubble trajectories for $\log_{10} M = -5.3$.

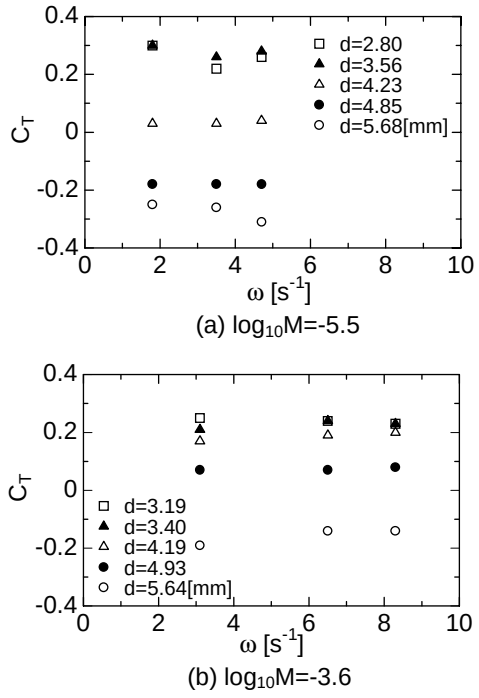

Fig. 5. Effects of liquid velocity gradient ω on C_T: (a) $\log_{10} M = -5.5$, (b) $\log_{10} M = -3.6$.

where $\boldsymbol{V}_R$ is the relative velocity ($=\boldsymbol{V}_G - \boldsymbol{V}_L$), $\boldsymbol{g}$ the acceleration due to gravity ($=(0, 0, -g)$) and C_D the drag coefficient, which was evaluated by (Tomiyama, Kataoka, Zun, & Sakaguchi, 1998b)

$$C_D = \beta \max\left[\min\left\{\frac{16}{Re}(1 + 0.15Re^{0.687}), \frac{48}{Re}\right\}, \frac{8}{3}\frac{Eo}{Eo+4}\right], \tag{8}$$

where β is a tuning factor to make calculated bubble velocities just equal to measured values, and Re the bubble Reynolds number defined by

$$Re = \frac{\rho_L |\boldsymbol{V}_R| d}{\mu_L}. \tag{9}$$

The value of C_T was adjusted so as to yield the best fits to the measured bubble trajectories. As shown in the solid curves in Fig. 4, we could confirm that all the measured trajectories were well reproduced with Eq. (7), which implies the validity of the employed assumption for the functional form of $\boldsymbol{F}_T$. It should be also noted that the acceleration of bubble velocity, $\mathrm{d}\boldsymbol{V}_L/\mathrm{d}t$, was negligibly small for all the measured bubbles, and thereby, even if we neglected the left-hand side of Eq. (7), there was no difference in the evaluated C_T. In other words, the value of the virtual mass coefficient, 0.5, in Eq. (7) had no substantial effects on the evaluation of C_T.

Fig. 5 shows thus evaluated net transverse lift coefficients C_T for two Morton number systems, (a) $\log_{10} M = -5.5$ and (b) $\log_{10} M = -3.6$. As shown in these figures, C_T takes positive values for small bubbles, whereas it takes negative values for large bubbles. In addition, C_T for a constant bubble diameter is not affected by the liquid velocity gradient ω and is more or less constant.

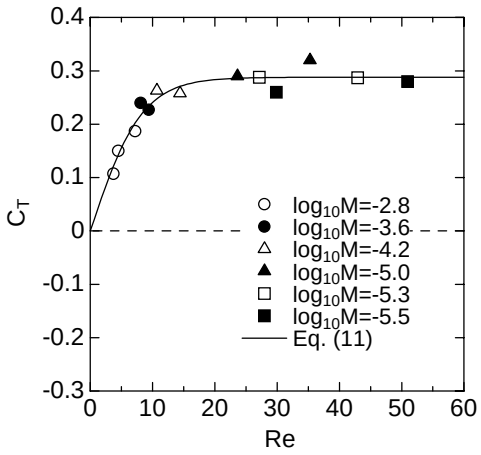

Fig. 6. C_T for small bubbles.

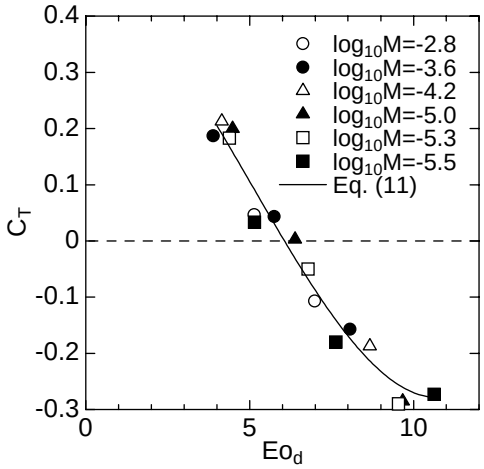

Fig. 7. C_T for large bubbles.

As shown in Figs. 6 and 7, we also found that C_T for small bubbles is well correlated with Re, whereas C_T for intermediate and large bubbles is a function of a modified Eötvös number Eo_d, which is defined by using the maximum horizontal dimension of a bubble as a characteristic length as follows:

$$Eo_d = \frac{g(\rho_L - \rho_G) d_H^2}{\sigma}. \tag{10}$$

The resulting empirical correlation of C_T is given by

$$C_T = \begin{cases} \min[0.288\tanh(0.121Re), f(Eo_d)] & \text{for } Eo_d < 4, \\ f(Eo_d) & \text{for } 4 \leqslant Eo_d \leqslant 10.7, \end{cases} \tag{11}$$

where

$$f(Eo_d) = 0.00105Eo_d^3 - 0.0159Eo_d^2 - 0.0204Eo_d + 0.474. \quad (12)$$

Eq. (11) yields $0 < C_T \leqslant 0.288$ for small bubbles migrating toward the wall, which coincides with available experimental data of C_T for small bubbles in an air–water system, e.g., $C_T = 0.3$ by Zun (1980) and $C_T = 0.25$ by Lance and Lopez de Berodano (1994). On the other hand, Eq. (11) gives negative values for large bubbles, and thereby large bubbles in a pipe flow would migrate toward the pipe center due to the net transverse lift force.

4. Application of C_T correlation to an air–water system

The proposed C_T correlation is based on the experimental data obtained in a high-viscosity system, so that in principle it is not applicable to a low-viscosity system such as air–water and vapor–water systems. However, as noted above, the correlation coincidentally yields the same value of C_T with experimental data for a small bubble in an air–water system. In view of this coincidence and the lack of C_T correlations for a low-viscosity system, it would be worth applying the proposed correlation to a bubble in an air–water system to examine whether or not it can explain the tendency of bubble lateral migration in a low-viscosity system.

4.1. Bubble lateral migration in a bubbly upflow

In an air–water system under atmospheric pressure and room temperature, the proposed C_T correlation yields the bubble diameter dependency shown in Fig. 8. To evaluate d_H in the definition of Eo_d, we made use of the following empirical correlation of the aspect ratio E for spheroidal bubbles in a fully contaminated system (Wellek, Agrawal, & Skelland, 1966):

$$E = \frac{d_V}{d_H} = \frac{1}{1 + 0.163Eo^{0.757}}, \quad (13)$$

where d_V is the maximum vertical dimension of a bubble.

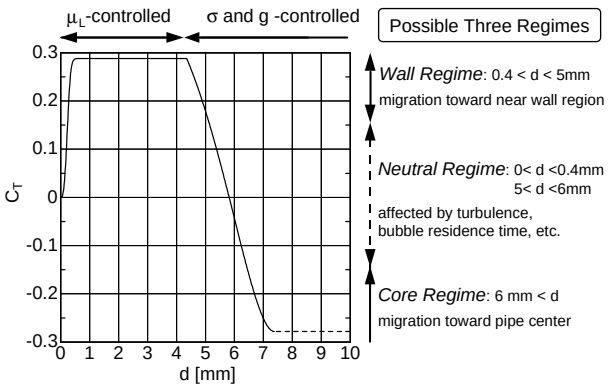

Fig. 8. C_T in an air–water system and postulated regimes of lateral migration.

For $d < 4.4$ mm, C_T is controlled by the bubble Reynolds number, i.e. by a viscous force. On the other hand, it is governed by the Eötvös number for $d > 4.4$ mm. C_T changes its sign at $d = 5.8$ mm from positive to negative. We can, therefore, postulate three regimes for the bubble lateral migration in a bubbly upflow in a vertical pipe. The first ($\varepsilon_1 \leqslant d < 5.8 - \varepsilon_2$ where ε_k (mm) is a small value) is a *wall regime* in which C_T takes a large positive value, and as a result, bubbles would migrate toward the pipe wall. The second ($d \geqslant 5.8 + \varepsilon_3$) is a *core regime* in which C_T takes a large negative value, and thereby bubbles would migrate toward the pipe center. The third ($5.8 - \varepsilon_2 \leqslant d < 5.8 + \varepsilon_3$ and $0 < d < \varepsilon_1$) is a *neutral or intermediate regime* in which the bubble lateral migration might be strongly affected by many other factors such as the magnitude of bulk liquid turbulence and a bubble residence time in a flow domain because the net transverse lift force in this regime keeps a low value due to the low magnitude of C_T.

Although the above-mentioned three regimes are based on the C_T correlation for single bubbles in viscous shear flows, they again coincide with available experimental data on radial void profiles in air–water turbulent bubbly upflows in vertical pipes. As an example, radial void profiles measured by Sakaguchi et al. (1996) are replotted in Fig. 9, in which R (=15.4 mm) is the pipe radius, r the radial coordinate, $\langle J \rangle$ the area-averaged volumetric flux, and $\langle \alpha_G \rangle$ the area-averaged void fraction. They measured the position and size of each bubble using an image processing method and classified bubbles into several groups in terms of their sizes. Then they obtained radial void profiles $\alpha_G(r, d)$ for each bubble group (A–F or a–f in the figure) and $\alpha_G(r)$ for all the bubbles (G or g). As shown in the figure, bubbles less than 5 mm (groups A–C or a–c) constitute the wall peaking, bubbles of 5–6 mm (group D or d) correspond to the intermediate profile, and bubbles larger than 6 mm (groups E and F or e and f) form the core peaking. Liu (1993) also measured bubble sizes and void profiles in air–water turbulent bubbly flows using a vertical pipe of $R = 28.6$ mm, and concluded that the critical bubble diameter causing the void profile transition from wall peaking to core peaking is about 5–6 mm. Though not to mention all, many experimental data have indicated that the profile transition in air–water bubbly flows occurs when bubbles are larger than about 5 mm (Grossetete, 1995; Zun, 1988). These facts imply that the net transverse lift coefficient in an air–water system is not so much different from the proposed C_T correlation.

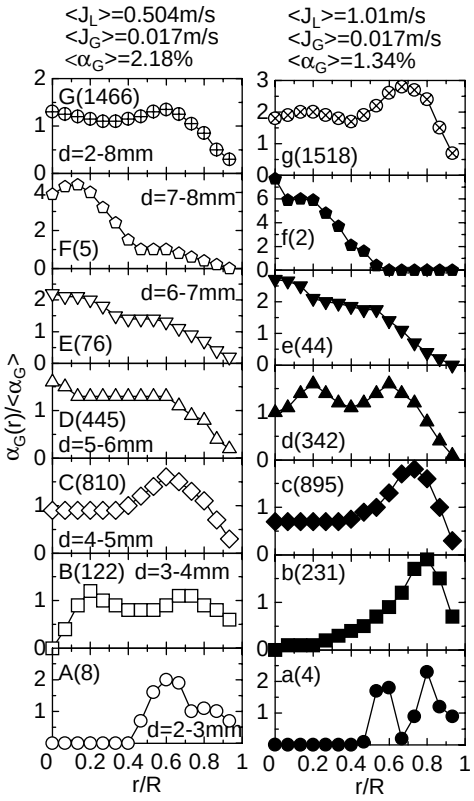

Fig. 9. Measured radial void profiles as a function of d; data are quoted from Sakaguchi et al. (1996).

4.2. Most probable radial position of a bubble in a turbulent bubbly upflow

Once we establish a reliable equation for the balance of lateral forces acting on a bubble, it would be possible to predict the most probable radial position r_{mp} of a bubble in an air–water bubbly flow in a vertical pipe. The lateral motion of a bubble in a turbulent bubbly flow would be, of course, affected by many factors such as the transverse lift force, bulk liquid turbulence, wall effect, non-rectilinear bubble path intrinsic to deformed bubbles, bubble collision and so on. However, for the purpose of evaluating the most probable radial position, we might be able to neglect the following effects: bubble collision, fluctuating bubble motion and bulk liquid turbulence, since these phenomena are more or less stochastic. In any case, a sort of restraining conditions to bubble lateral migration is indispensable to account for wall effects. At this stage of examining whether or not the C_T correlation can explain the tendency of r_{mp} in a turbulent bubbly flow, we might be able to employ a wall force model proposed by Tomiyama et al. (1995) as one representation of wall effects. Other possible way to express the restraining condition would be an extended mixing length theory that accounts for shear- and bubble-induced turbulence (Zun, 1985).

Then we can set up the following balance of lateral forces acting on a bubble in a pipe flow, which is based on the net

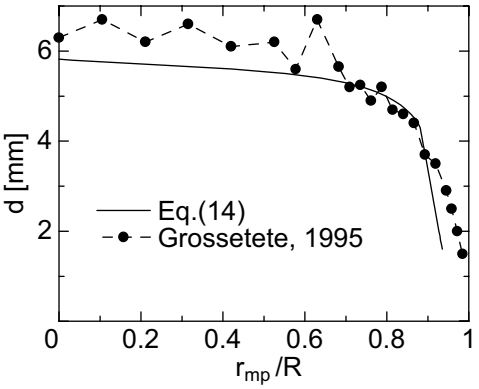

Fig. 10. Relation between calculated r_{mp} and d; the closed circles are the radial profile of mean bubble diameter in a turbulent bubbly upflow measured by Grossetete (1995).

transverse lift force model, Eqs. (6) and (11), and a wall force model proposed by Tomiyama et al. (1995):

$$F_T + F_W = \frac{\pi d^3}{6} \times \left(-C_T \rho_L V_R \frac{\partial V_L}{\partial r} - C_W f(r) \frac{1}{2} \rho_L V_R^2 \right) = 0, \tag{14}$$

where F_W denotes the wall force, V_R the relative velocity between the bubble and liquid, V_L the axial component of the liquid velocity, C_W the empirical coefficient of wall force, a typical value of which is about 0.1 for bubbles in an air–water turbulent bubbly flow (Tomiyama, Miyoshi, Tamai, Zun, & Sakaguchi, 1998a), and $f(r)$ is given by

$$f(r) = d \left[\frac{1}{(R-r)^2} - \frac{1}{(R+r)^2} \right]. \tag{15}$$

For an air–water system, the relative velocity of bubbles larger than 1.3 mm in equivalent diameter can be evaluated by (Tomiyama et al., 1998b)

$$V_R = \sqrt{\frac{2\sigma}{\rho_L d} + \frac{(\rho_L - \rho_G) g d}{2\rho_L}} \tag{16}$$

and the mean liquid velocity profile $V_L(r)$ is given by

$$V_L(r) = 1.2 \frac{\langle J_L \rangle}{1 - \langle \alpha_G \rangle} \left(1 - \frac{r}{R} \right)^{1/7}. \tag{17}$$

By substituting Eqs. (15)–(17) and the C_T correlation into Eq. (14), we can set up a nonlinear algebraic equation with respect to r, the solution of which is the most probable radial position of a bubble in a pipe flow. As an example, the above lateral force balance was applied to an experiment conducted by Grossetete (1995): an air–water turbulent bubbly upflow, $R = 19.05$ mm, $\langle J_G \rangle = 0.0917$ m/s, $\langle J_L \rangle = 0.526$ m/s, $\langle \alpha_G \rangle = 0.131$ and $1 < d < 7$ mm at $z/R = 310$ where z is the axial elevation from an air–water mixing section. The calculated most probable radial position r_{mp} of a bubble is shown in Fig. 10 together with the measured

radial profile of mean bubble diameter. It should be noted that the measured data do not directly correspond to the most probable radial position of a bubble. The data just show a radial distribution of mean bubble diameter in the turbulent bubbly flow consisting of bubbles ranging from about 1 to 7 mm in equivalent diameter. Therefore, it might be inappropriate to make a direct comparison between the calculation and experiment. Nonetheless, both data show similar tendencies such as (1) bubbles less than about 4.5 mm are apt to flow in the near-wall region, (2) bubbles ranging from 4.5 to 5.5 mm flow around $r/R = 0.8$ and (3) bubbles larger than 5.5 mm tend to flow in the core region, i.e. $r/R < 0.7$. Consequently, we could confirm that it is possible to predict the trend of r_{mp} in an air–water turbulent bubble flow by using the proposed C_T correlation and the wall force model. However, it should be noted that even if r_{mp} is well predicted by the simple force balance, it does not imply the validity of the C_T correlation for bubbles in an air–water turbulent flow. The net transverse lift coefficient in the turbulent bubbly flow must be affected by many other factors and take a different value from the value given by the C_T correlation. Further studies on bubble lateral migration are therefore indispensable to establish a C_T model applicable to low-viscosity systems.

5. Conclusions

Trajectories of single air bubbles in simple shear flows of glycerol–water solution were measured to evaluate transverse lift force acting on a bubble. Experiments were conducted under the conditions of $-5.5 \leqslant \log_{10} M \leqslant -2.8$, $1.39 \leqslant Eo \leqslant 5.74$ and $0 \leqslant |\mathrm{d}V_L/\mathrm{d}y| \leqslant 8.3\ \mathrm{s}^{-1}$, where M is the Morton number, Eo the Eötvös number and $\mathrm{d}V_L/\mathrm{d}y$ the velocity gradient of the simple shear flow of liquid. A net transverse lift coefficient C_T was evaluated by making use of all the measured trajectories and an equation of bubble motion. As a result, the following conclusions were obtained:

(1) C_T for small bubbles is well correlated with the bubble Reynolds number, whereas C_T for larger bubbles is a function of a modified Eötvös number based on the maximum horizontal dimension of a bubble as a characteristic length. The resulting C_T correlation is given by Eqs. (11) and (12).
(2) The critical bubble diameter causing the radial void profile transition from wall peaking to core peaking in an air–water bubbly upflow evaluated by the C_T correlation coincides with available experimental data.

Notation

C_D	drag coefficient
C_{LF}	lift coefficient
C_T	net transverse lift coefficient
C_{TL}	transverse lift coefficient
C_W	wall effect coefficient
d	sphere-volume equivalent diameter of a bubble
D	gap width
d_H	maximum horizontal dimension of a bubble
d_V	maximum vertical dimension of a bubble
$\mathrm{d}V_L/\mathrm{d}y$	velocity gradient of a simple shear flow
Eo	Eötvös number
Eo_d	modified Eötvös number
$\boldsymbol{F}_{LF}$	shear-induced lift force
$\boldsymbol{F}_T$	net transverse lift force
$\boldsymbol{F}_{TL}$	transverse lift force due to a slanted wake
$\boldsymbol{F}_W$	wall force
$\boldsymbol{g}$	acceleration due to gravity
$\langle J \rangle$	area-averaged volumetric flux
M	Morton number
r	radial coordinate
R	pipe radius
Re	bubble Reynolds number
r_{mp}	most probable radial position of a bubble
$\boldsymbol{V}$	velocity
$\boldsymbol{V}_R$	relative velocity
y	horizontal coordinate
y^*	dimensionless horizontal coordinate ($=y/D$)
z	vertical coordinate
z^*	dimensionless vertical coordinate ($=z/D$)

Greek letters

$\langle \alpha_G \rangle$	area-averaged void fraction
β	tuning factor for drag force
ε	small value
μ	viscosity
ρ	density
σ	surface tension
ω	magnitude of velocity gradient

Subscripts

G	gas phase
L	liquid phase

Appendix.

All the measured trajectories, shapes, sphere-volume equivalent diameters and maximum horizontal dimensions of single bubbles are shown in Figs. 11 and 12. As shown in Fig. 12, bubbles exhibit intrinsic fluctuation of rise path for $\log_{10} M \leqslant -5.5$. This is the main reason why we could not conduct experiments for systems with much lower liquid viscosity. Fluid properties in each Morton number system are summarized in Table 1.

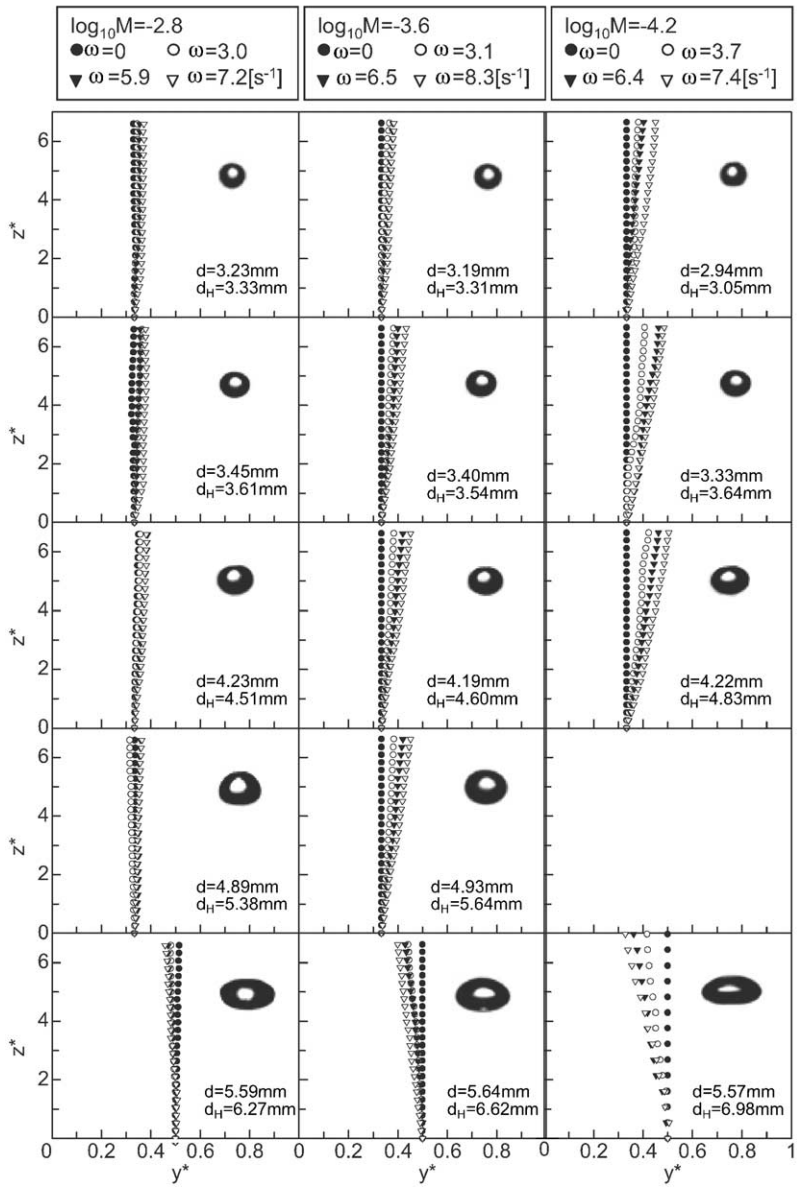

Fig. 11. Measured bubble trajectories for $\log_{10} M = -2.8, -3.6$ and -4.2.

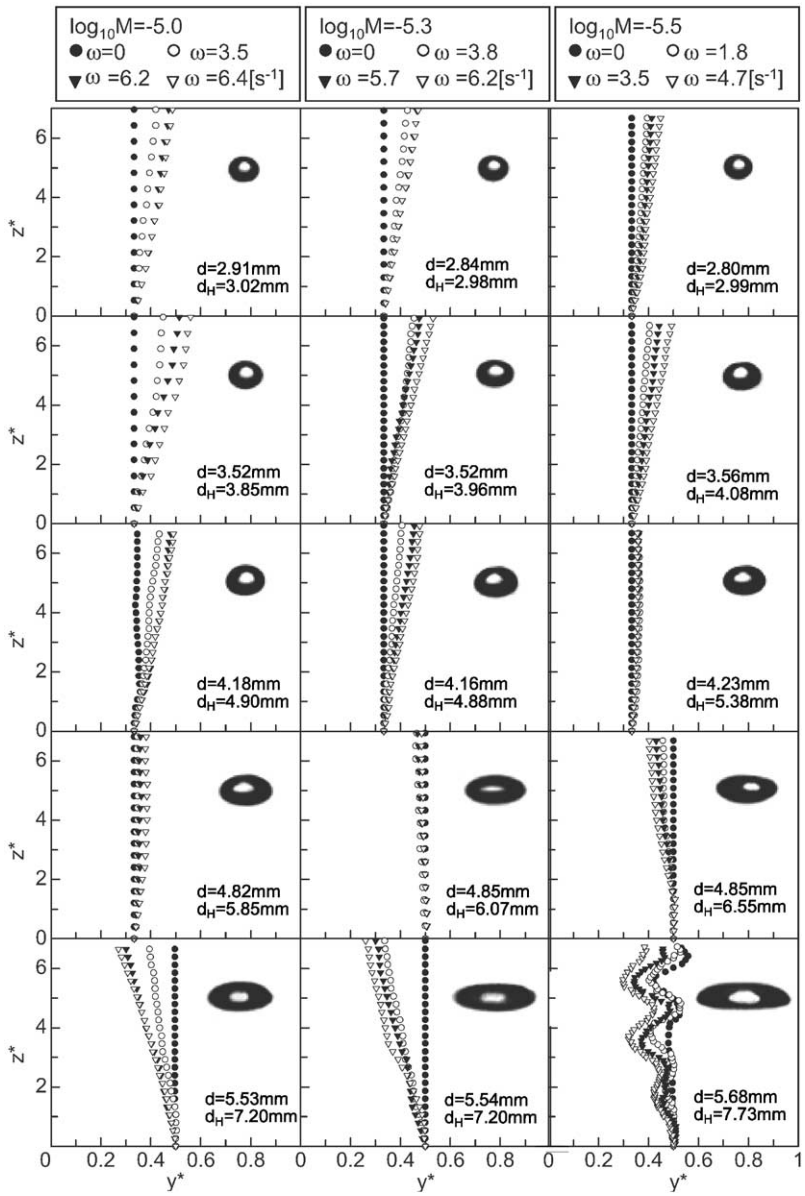

Fig. 12. Measured bubble trajectories for $\log_{10} M = -5.0, -5.3$ and -5.5.

Table 1
Measured fluid properties

$\log_{10} M$	− 2.8	− 3.6	− 4.2	− 5.0	− 5.3	− 5.5
ρ_L (kg/m^3)	1209	1180	1165	1166	1154	1150
μ_L (kg/m s)	0.089	0.053	0.038	0.022	0.019	0.018
σ (N/m)	0.067	0.063	0.064	0.061	0.061	0.063

References

Auton, T. R. (1987). The lift force on a spherical body in a rotational flow. *Journal of Fluid Mechanics*, *183*, 199–218.

Drew, D., & Lahey Jr., R. T. (1987). The virtual mass and lift force on a sphere in a rotating and straining flow. *International Journal of Multiphase Flow*, *13*, 113–121.

Grossetete, C. (1995). Experimental investigation of void profile development in a vertical cylindrical pipe. In A. Serizawa, T. Fukano, & J. Bataille (Eds.), *Advances in multiphase flow* (pp. 333–346). Amsterdam: Elsevier.

Kariyasaki, A. (1987). Behavior of a gas bubble in a liquid flow with a linear velocity profile. *Transactions of Japan Society of Mechanical Engineers, Series B*, *53*, 744–749 (in Japanese).

Lance, M., & Lopez de Berodano, M. (1994). Phase distribution phenomena and wall effects in bubbly two-phase flows. In G. F. Hewitt, J. H. Kim, R. T. Lahey Jr., J. M. Delhaye, & N. Zuber (Eds.), *Multiphase science and technology*, Vol. 8, (pp. 69–123). New York: Begell House Inc.

Liu, T. J. (1993). Bubble size and entrance length effects on void development in a vertical channel. *International Journal of Multiphase Flow*, *19*, 99–113.

Sakaguchi, T., Ijiri, H., Tabasaki, M., & Shakutsui, H. (1996). Radial distribution of volume fraction of gas phase in gas-liquid two-phase bubbly flow in a certical pipe. *Japanese Journal of Multiphase Flow*, *10*(4), 389–396 (in Japanese).

Serizawa, A., & Kataoka, I. (1994). Dispersed flow-I. In G. F. Hewitt, J. H. Kim, R. T. Lahey Jr., J. M. Delhaye, & N. Zuber (Eds.), *Multiphase science and technology*, Vol. 8 (pp. 125–194). New York: Begell House Inc.

Tomiyama, A., Kataoka, I., Zun, I., & Sakaguchi, T. (1998b). Drag coefficients of single bubbles under normal and micro gravity conditions. *JSME International Journal, Series B*, *41*, 472–479.

Tomiyama, A., Miyoshi, K., Tamai, H., Zun, I., & Sakaguchi, T. (1998a). A bubble tracking method for the prediction of spatial-evolution of bubble flow in a vertical pipe, *on CD-ROM of third international conference of multiphase flow, ICMF'98*, Lyon (pp. 1–8).

Tomiyama, A., Sou, A., Zun, I., Kanami, N., & Sakaguchi, T. (1995). Effects of Eötvös number and dimensionless liquid volumetric flux on lateral motion of a bubble in a laminar duct flow. In A. Serizawa, T. Fukano, & J. Bataille (Eds.), *Advances in multiphase flow* (pp. 3–15). Amsterdam: Elsevier.

Tomiyama, A., Zun, I., Sou, A., & Skaguchi, T. (1993). Numerical analysis of bubble motion with the VOF method. *Nuclear Engineering Design*, *141*, 69–82.

Wellek, R. M., Agrawal, A. K., & Skelland, A. H. P. (1966). Shapes of liquid drops moving in liquid media. *A.I.Ch.E. Journal*, *12*, 854–862.

Zun, I. (1980). Transverse migration of bubbles influenced by walls in vertical bubbly flow. *International Journal of Multiphase Flow*, *6*, 583–588.

Zun, I. (1985). The role of void peaking in vertical two-phase bubbly flow, *Second international conference on multi-phase flow*, London (pp. 127–139). Cranfield: BHRA The fluid engineering center.

Zun, I. (1988). Transition from wall void peaking to core void peaking in turbulent bubbly flow. *Proceedings of transient phenomena in multiphase flow*, *ICHMT international seminar*, Dubrovnik, Croatia (pp. 225–233).